J. Fluid Mech. (2021), *vol*. 908, A1. © The Author(s), 2020.
Published by Cambridge University Press
doi:10.1017/jfm.2020.821

Transport of particles in a turbulent rough-wall pipe flow

L. Chan[1],†, T. Zahtila[1], A. Ooi[1] and J. Philip[1]

[1]Department of Mechanical Engineering, The University of Melbourne, Victoria 3010, Australia

(Received 20 January 2020; revised 22 July 2020; accepted 21 September 2020)

Dense, small particles suspended in turbulent smooth-wall flow are known to migrate towards the wall. It is, however, not clear if the particle migration continues in a rough-wall flow and what the responsible mechanism is, especially with changing roughness parameters. Here, we address this using direct numerical simulation of a turbulent pipe flow of a fixed friction Reynolds numbers and changing the roughness size as well as the Stokes number of the particles. The transport and deposition mechanisms of particles are segregated into three different regimes dictated by the Stokes number. Particles with small Stokes number follow the carrier fluid and are affected by the turbulent structures of the rough wall. Flow separation in the wake of the roughness and stagnant flow in the trough of the roughness causes these particles to be trapped in the roughness canopy. Particles with very large Stokes number, on the other hand, are attracted to the wall due to turbophoresis and collide with the rough wall where the frequency of wall collision increases with increasing Stokes number. These ballistic particles are unaffected by the turbulent fluctuations of the flow and their trajectory is determined by the roughness topography. At intermediate Stokes numbers, the transport of the particles is influenced by both the wall collisions and also the turbulent flow. Particles in this range of Stokes number occasionally collide with the wall and are entrained by the turbulent flow. In this regime, the particles may have a mean streamwise velocity that is larger than the bulk flow rate of the fluid. Finally, we observe that bulk particle velocity scale better with a time scale based on the roughness elements rather than the usual viscous time scale.

Key words: pipe flow boundary layer, particle/fluid flow

1. Introduction

The transport of particulates in an internal flow has various applications in engineering. Here, we are particularly motivated by the movement of heavy solid particles in air inside turbulent pipe flows. The flow within smooth wall-bounded flows have received considerable attention in the literature. The focus of this paper, however, is on the motion of dense point particles in turbulent pipe flows with a periodic three-dimensional wall roughness. Our interest is in understanding the influence of particles with different inertia and varying roughness parameters on the particle dynamics. In the following we first briefly review the salient features of particle dynamics in smooth turbulent wall flows, and then survey the rough wall results.

† Email address for correspondence: lzhchan@unimelb.edu.au

The dominant phenomenon of dispersed particles in a turbulent flow with smooth walls is their transport towards, and accumulation at, the walls (e.g. Guha 1997). This arises from the interaction of a particles' inertia and the fluid's turbulent eddies (e.g. Young & Leeming 1997). Particles of all sizes accumulate on smooth walls at different time scales and this is termed 'deposition.' The particles' inertia is quantified by the particle relaxation time, $\tau_p = \rho_p d_p^2/(18\rho\nu)$, where ρ_p and d_p are the density and diameter of the particles and ρ and ν are the density and the kinematic viscosity of the fluid. In wall-bounded flows, the particle relaxation time is non-dimensionalised with the viscous time scale $\tau_f = \nu/U_\tau^2$ ($U_\tau = \sqrt{\tau_w/\rho}$ is the friction velocity and τ_w is the total wall stress – to be defined later), and this parameter is known as the particle Stokes number $St^+ = \tau_p/\tau_f$. In the limit of small Stokes number, particles deposit at the wall due to turbulent diffusion. As the particles' St^+ increases, their inability to follow curved streamlines increases their deposition rate by several orders of magnitude.

The recognition of the transport of particles being essentially linked to the turbulent flow structures is widely acknowledged by statistics collected from direct numerical simulation (DNS) and experimental works, for example of Rouson & Eaton (2001), Fessler, Kulick & Eaton (1994) and Kulick, Fessler & Eaton (1994). The flow mechanisms in the buffer region that govern the migration of particles towards smooth walls includes sweeps, which increase the likelihood that a particle will firstly reach the wall (e.g. Marchioli & Soldati 2002). Actually, for small and moderate Stokes numbers, the probability that a particle with a wall-directed velocity at height $y^+ = 11$ is engulfed in a sweep exceeds 95 % and the probability that a wall-fleeing particle at this height is ejection-entrained exceeds 90 %. Once in the near-wall region, preferential segregation of particles is in regions of lower streamwise velocity and these segregations appears as long streamwise aligned streaks as observed by Sardina *et al.* (2012*a*). Thus, wall accumulation in smooth wall flows is not simply a matter of particles reaching the wall, but further is conditioned on their sampling of fluid events to organise in the near-wall region, preventing efficient ejection mechanisms.

Modification to this process by rough walls is of practical relevance as most engineering surfaces are not hydrodynamically smooth, and contain surface defects and irregularities due to the manufacturing process. Roughness increases drag and causes a decrease in the viscous scaled mean velocity profile. This downward shift in the mean velocity is quantified by the Hama roughness function (ΔU^+, which is the reduction in the mean streamwise velocity in the inertial region compared to a smooth pipe flow). The near-wall turbulent structures of the flow are also modified by the roughness topography. Numerical and laboratory experiments of turbulent flow over rough walls have found that roughness reduces the streamwise length of the near-wall structures (Orlandi & Leonardi 2006; Volino, Schultz & Flack 2007; Chan *et al.* 2018), increases the inclination angle of the coherent structures (Krogstad & Antonia 1994; Coceal *et al.* 2007) and weakens these structures (MacDonald *et al.* 2016; Chan *et al.* 2018) which are responsible for the near-wall turbulence regeneration mechanism (Hamilton, Kim & Waleffe 1995).

Changes in the turbulent structures can greatly affect the transport of particles. Numerical works of Milici *et al.* (2014) in a channel flow found that the preferential accumulation of particles observed in a smooth wall is not observed in a rough wall. They attributed the different deposition mechanism in a rough-wall flow as due to the different near-wall turbulent structures where heavier particles ($St^+ > 10$) are more likely to be entrained by high-velocity wall-fleeing ejection events. This led to an increased concentration at the centre of the channel. Subsequent work by De Marchis *et al.* (2016) concluded that turbophoresis disappears in a turbulent rough-wall-bounded flow as the roughness destroys the near-wall streaky structures.

In addition to turbulence, the importance in particle wall collision can not be understated in a rough-wall-bounded flow. An experimental study conducted by Kussin & Sommerfeld (2002) in a rough-wall channel found that roughness reduces the efficiency of particle transport by the continuum phase due to the irregular wall bouncing and increases the wall collision frequency. Benson, Tanaka & Eaton (2004) also reported similar findings where roughness reduces the streamwise particle velocities by up to 40 %. The particle velocities were also more uniform across the rough channel compared to the smooth channel. Stochastic modelling of the particle–rough-wall collision have been developed to emulate the rebound effects of a rough wall. In these models, the rebound trajectory of the particles is calculated by introducing a smooth virtual inclined wall with a characteristic chosen angle (Sommerfeld 1992). A simplistic wall model has been used by Vreman (2007) in a turbulent pipe flow and is found to be an important factor to obtain agreement with experimental data. However, these virtual wall models do not take into account the height of the roughness (Sommerfeld & Huber 1999; Konan, Kannengieser & Simonin 2009), which is an important parameter because fluid velocity in the vicinity of the crest is high and the particles would sample different turbulent structures compared to the trough of the roughness. In this study, we will explicitly evaluate the wall collision and rebound processes of the particles rather than using a virtual wall modelling. We note that the numerical simulation of two-phase flows in a turbulent pipe has been conducted mostly for a smooth wall (Uijttewaal & Oliemans 1996; Oliveira, van der Geld & Kuerten 2017) or with modelled roughness (Vreman 2007). While there has been experimental work on two-phase rough-wall flows, numerical simulation of particle laden turbulent flows over a rough surface is limited (Chang & Scotti 2003; Milici *et al.* 2014) and to the best of the authors' knowledge, none are available in a pipe with explicitly gridded (or resolved) roughness.

In this paper, we will be investigating both the wall collision effects and the influence of the rough-wall turbulent structures on the particle deposition and transport mechanisms in a pipe. The roughness in the pipe consists of three-dimensional sinusoidal roughness with a staggered arrangement. A body fitted grid is used to mesh the roughness topography and the particle–wall collision is directly calculated without the need for stochastic modelling. This roughness is chosen as the turbulent flow over this idealised, homogeneous roughness has been thoroughly investigated previously with different roughness heights, wavelengths and Reynolds numbers (Chan *et al.* 2015, 2018). While most numerical simulations of rough-wall flows with particles have only simulated a single roughness case, here, we alter the height of the roughness to systematically investigate the importance of the roughness topography on the transport and wall accumulation of particles. Eight sets of particles with a Stokes number spanning three decades ranging from dust particles to millimetre sized gold particles in the air are simulated. The results from the turbulent flow over sinusoidal roughness coupled with the wide range of particle Stokes numbers allow us to uncover the different particle transport and deposition mechanisms, which might be dominated by turbulent flow structures or wall collisions or a combination of both. Although the changes to the flow due to the particles are important, it is not the primary interest here. Dilute particle concentration is naturally the first step, where one-way coupling is a reasonable assumption.

The cylindrical coordinate notation is used for the pipe where x, r, θ are the streamwise, radial and azimuthal directions, respectively. Capitalised variables are time averaged and variables with the $^+$ superscript are viscous scaled, where $t^+ = U_\tau^2 t/\nu$, $l^+ = U_\tau l/\nu$ and $u^+ = u/U_\tau$ are the viscous time scale, length scale and velocity scale respectively.

2. Computational set-up

The Eulerian–Lagrangian method is used to conduct the particle laden pipe flow simulations. The continuity and Navier–Stokes equations which govern the motion of the fluid are solved and written as below:

$$\nabla \cdot \boldsymbol{u} = 0, \tag{2.1}$$

$$\rho \frac{\mathrm{D}\boldsymbol{u}}{\mathrm{D}t} = -\nabla p + \mu \nabla^2 \boldsymbol{u} + F_x \boldsymbol{i}, \tag{2.2}$$

where $\boldsymbol{u}$ is the velocity vector, p is the pressure fluctuation, ρ and $\mu = \rho\nu$ are the density and dynamic viscosity of the fluid, respectively, and $F_x(t)$ is the time varying body force in the $\boldsymbol{i}$ (or x) direction to ensure a constant mass flux in the pipe. Only the effects of the fluid on the particles are considered (one-way coupling) and the governing equations for the Lagrangian point particle system are as below:

$$\frac{\mathrm{d}\boldsymbol{x}^p}{\mathrm{d}t} = \boldsymbol{u}^p, \tag{2.3}$$

$$m_p \frac{\mathrm{d}\boldsymbol{u}^p}{\mathrm{d}t} = \frac{m_p}{\tau_p}\left(1 + \frac{1}{6}Re_p^{2/3}\right)(\boldsymbol{u} - \boldsymbol{u}^p), \tag{2.4}$$

where m_p is the mass of the particle, $\boldsymbol{u}^p$ is the velocity of the particle and $Re_p = d_p|\boldsymbol{u} - \boldsymbol{u}^p|/\nu$ is the particle Reynolds number and the drag correlation developed by Putnam (1961) is used.

The density ratio of the particle to the carrier phase ρ_p/ρ is set to be 10 000 so that the drag force is the only significant force acting on the particles in the absence of gravity (e.g. Armenio & Fiorotto 2001; Bagchi & Balachandar 2004; Burton & Eaton 2005). A density ratio of 10 000 was chosen so that particles with larger St^+ would still be within the constraint of the point particle method where the particle diameter has to be smaller than the Kolmogorov scale (Maxey & Riley 1983). We have carried out additional simulations in our rough-wall pipe flow with $St^+ = 100$ but with density ratio $\rho_p/\rho = 1000$, and the concentration distribution is similar to $\rho_p/\rho = 10\,000$ (not shown in this manuscript). The comparison is made here because many researchers have used $\rho_p/\rho = 1000$ (e.g. Picano, Sardina & Casciola 2009; Milici *et al.* 2014; De Marchis & Milici 2016).

Gravitational effects are important for particles with larger St^+, however, are not included to avoid any added complexity when comparing the transport of particles in smooth- and rough-wall flows, as has been neglected in previous rough-wall studies (e.g. Milici *et al.* 2014; De Marchis & Milici 2016). The importance of the gravitational force is quantified by the particle Froude number, $Fr_p = U_b/(g\tau_p)$ introduced by Sardina *et al.* (2012*b*). In the present study, particles with $St^+ \leq 200$ have Fr_p values that are larger than 1 (assuming $g = 9.81$ ms^{-2}, Fr_p ranges from 294 to 0.29 for $1 \leq St^+ \leq 1000$) and consequently the effects of gravity are minimal for the smaller particles where $Fr_p \gg 1$. The lift force is also neglected as it is deemed to be small, although it is found to have a significant effect on the concentration of particles in the near-wall region (Costa, Brandt & Picano 2020). A discussion on the importance of the lift force is included in appendix B where the lift force is found to have a minor effect on the distribution of particles in a rough wall.

The simulations were conducted using the open-source code OpenFOAM (Weller *et al.* 1998). The barycentric tracking algorithm is used to track the particles and fluid quantities are interpolated to particle coordinates by means of inverse distance weights with linear

interpolation from the Eulerian grid. The ordinary differential equations associated with particle motion are integrated in time through an implicit Euler scheme. A particle–wall collision is defined to have occurred when the point particle crosses a cell face located on the boundary of the domain, and for the perfectly elastic case, the particle velocity in the wall-normal direction is then reversed (Ambrosino 2011). Since the particle–wall collision splits the normal and parallel components of motion to the boundary face, there is no difference in treatment of smooth-wall or rough-wall geometries. Particle–particle interactions are neglected as the particle concentrations are assumed to be dilute.

Cell-centred variables are linearly interpolated to face centres followed by a standard finite volume procedure with non-orthogonal correction for gradients at face centres. The choice of temporal discretisation is the second-order accurate backward Euler scheme. OpenFOAM is a collocated grid solver and, to remove spurious pressure oscillations, careful discretisation is required of the pressure gradient and the Laplacian of pressure that appears in the pressure equation. Avoiding oscillations on non-staggered grids was first suggested by Rhie & Chow (1983), and constitutes a remedy for the error term that arises from an inconsistent stencil for the gradient and Laplacian operators. This requirement to avoid spurious oscillations is satisfied in OpenFOAM by applying Gauss' theorem to the Laplacian term that arises in the pressure equation and by interpolating variables stored at cell centres to cell faces. A detailed account of Rhie–Chow correction in OpenFOAM is available from Kärrholm (2006). The OpenFOAM continuous phase results are verified with our previous simulations (Chan *et al.* 2015) and show good agreement (see appendix A).

The simulation is conducted in a rough-wall pipe with a domain length of $L_x = 4\pi R_0$, where R_0 is the mean radius of the pipe. This domain length has found to be sufficiently long to obtain converged second-order fluid statistics in a smooth-wall pipe (Chin *et al.* 2010) and the presence of roughness decreases the streamwise length of the largest structures (Chan *et al.* 2018), thus avoiding the need for a longer domain. The sinusoidal roughness elements are governed by the following equation:

$$R(x,\theta) = R_0 + h\cos\left(\frac{2\pi x}{\lambda_x}\right)\cos\left(\frac{2\pi R_0\theta}{\lambda_s}\right). \tag{2.5}$$

Here, h is the roughness semi-amplitude (half of the peak-to-trough height) and λ_x and λ_s are the wavelengths of the roughness elements in the streamwise and azimuthal directions. For all of the rough cases simulated, $\lambda_x = \lambda_s = \lambda$. The virtual origin of the wall ($y = 0$) is set to be R_0, which is also the mean radius of the pipe, and it leads to a good collapse in the statistics in the outer region of the flow (Chan *et al.* 2015). Simulations were conducted at a friction Reynolds number of $Re_\tau = U_\tau R_0/\nu \approx 180$ where, as mentioned before, $U_\tau = \sqrt{\tau_w/\rho}$ is the friction velocity. Here, τ_w is the total wall stress, and along with a hydraulic radius $R_h \equiv \sqrt{V/(\pi L_x)}$ with V the total pipe volume occupied by the fluid, leads in our rough-wall case to include both viscous and pressure stress in τ_w, i.e.

$$\begin{aligned}\tau_w &\equiv -\frac{\int_S (-pn_x + \mu\boldsymbol{n}\cdot\nabla\boldsymbol{u})\,\mathrm{d}S}{(2\pi R_h)L_x}, \quad \text{which using (2.2) becomes}\\ &= \frac{\rho F_x V}{(2\pi R_h)L_x} = \frac{\rho F_x R_h}{2}.\end{aligned} \tag{2.6}$$

Here, S is the pipe surface area bounding V, $\boldsymbol{n}$ the outward surface normal and $\mu = \rho\nu$ the dynamic viscosity (e.g. Chan *et al.* 2015). We note that, in the smooth-wall case, (2.6)

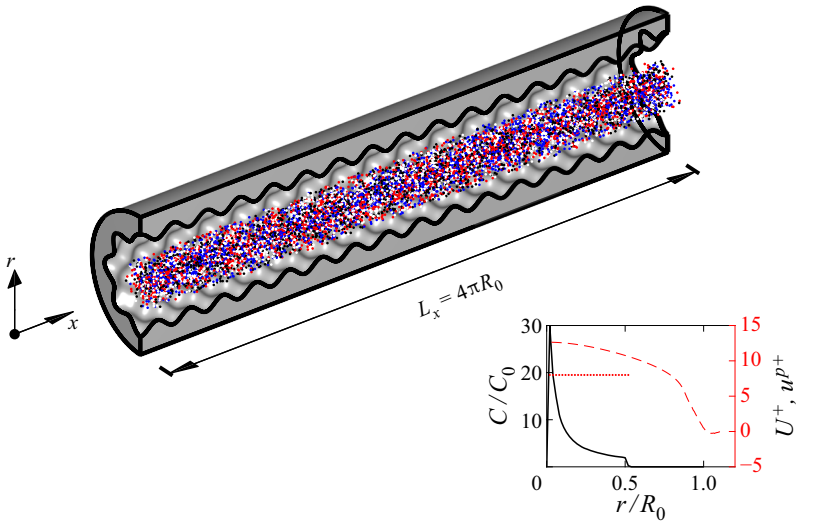

FIGURE 1. Sketch of the computational domain of the rough-wall pipe with $h^+ = 20$ and the initial positions of the particles. The different colours illustrate the particles with different St^+ and only 10 000 particles are shown for clarity. The x-axis is in the streamwise direction and the radial distance, r, is measured from the centre of the pipe; L_x is the length of the pipe. The plot shows the initial concentration of the particles (solid black line) and the injected velocity of the particles u^{p+} (red dotted line) relative to the mean velocity profile of the fluid U^+ (red dashed line).

reduces to the usual $\tau_w = \mu\, \mathrm{d}U/\mathrm{d}y$, with $y := R_0 - r$ being the normal distance from the wall.

A total number of 5 068 800 cells were used for each case and the average resolution of the cells at the wall are $\Delta y^+ \approx 0.22$, $r\Delta\theta^+ \approx 4.71$ and $\Delta x^+ \approx 5.89$. This corresponds to a grid spacing to Kolmogorov length scale of $\Delta y/\eta \approx 0.14$, $r\Delta\theta/\eta \approx 2.94$ and $\Delta x/\eta \approx 3.68$ at the wall where $\eta = (\nu^3/\epsilon)^{1/4}$ is the Kolmogorov scale (which is smallest in the near-wall region) and $\epsilon = 2\nu\overline{s'_{ij}s'_{ij}}$ is the dissipation, where $s'_{ij} = (\partial u'_i/\partial x_j + \partial u'_j/\partial x_i)/2$ is the strain rate tensor. The cells are equally spaced in the streamwise direction and in the azimuthal direction at the pipe walls. A grid geometric stretching is applied in the wall-normal direction with a cell-to-cell expansion ratio of less than 1.05. A sufficiently small time step was used (tabulated in table 2) to ensure that the maximum Courant number is less than 0.6. While the simulations have been conducted at a low Reynolds number, it is expected that the physics of the near-wall region, which is the focus of this study, will not be greatly different at higher Reynolds number. The continuous phase is simulated until reaching a fully developed state before particles are released to the flow. Eight sets of particles ranging from $St^+ = 1$ to 1000 each with 200 000 particles, are randomly distributed in the core of the pipe $0 < r/R_0 < 0.55$ (see figure 1), and the initial velocity of the particles is set to be equal to the fluid's bulk velocity for faster particle statistics convergence. Eight particle diameters and four roughness heights provide us with 32 cases to systematically study the effect of roughness induced turbulence on particles. The two-phase flow simulation is run for at least $\Delta t^+ \approx 10\,800$ to reach a statistically steady state, independent of the initial conditions and particle statistics are averaged for at least $\Delta t^+ > 720$. Table 1 shows the summary of the range of particles in the flow, whereas table 2 provides details of the rough-wall pipes.

St^+	1	10	50	100	200	300	500	1000
d/R_0	0.00024	0.00075	0.00167	0.00236	0.00333	0.0041	0.00527	0.00745
d^+	0.042	0.134	0.300	0.424	0.600	0.735	0.949	1.342

TABLE 1. Summary of the different particle types used in the simulation.

Cases	Re_τ	Re_{cl}	Re_D	R_0/h	λ/R_0	h/λ	k_a^+	k_{rms}^+	ES	ΔU^+	Δt^+
Sm	180	7043	5357	—	—	—	0.00	0.0	0.00	0.00	0.072
*h*05	180	6548	4896	36	0.785	0.035	2.03	2.5	0.09	1.38	0.072
*h*10	180	5717	4122	18	0.785	0.071	4.05	5.0	0.18	3.71	0.072
*h*20	180	4550	2880	9	0.785	0.141	8.11	10.0	0.36	7.08	0.036

TABLE 2. Roughness characteristics and mean flow properties; k_a^+ and k_{rms}^+ are the average and root-mean-square roughness heights and ES is the effective slope; ΔU^+ is the Hama roughness function and Δt^+ is the viscous scaled time step.

3. Smooth vs rough wall

A visual comparison between the instantaneous distribution of particles with $St^+ = 1$ and 100 for the unwrapped smooth- and rough-wall pipe ($h^+ = 20$) is presented in figure 2. In figure 2(*a*), we observe that the particles with $St^+ = 1$ (in white) are randomly distributed throughout the domain whereas the heavy particles with $St^+ = 100$ (in black) accumulate at the wall. The segregation between these two different particles is clearly illustrated in the streamwise–wall-normal slice in (*i*). This phenomenon of particle migration to the smooth wall for inertial particles is due to turbophoresis (particle migration due to turbulence) and is well studied in the literature (e.g. Reeks 1983; Guha 1997; Balachandar & Eaton 2010). On the other hand, for the rough-wall case, particles with $St^+ = 100$, which are inertial, collide and bounce off the wall and are homogeneously distributed throughout the pipe, as observed in the streamwise–wall-normal plane at different azimuthal slices (figure 2*ii–iv*).

Figure 3 shows the plot of the normalised particle concentration (C/C_0) against the viscous scaled wall-normal height comparing the (*a*) smooth-wall and (*b*) rough-wall cases, and also comparing the effects of different particle Stokes number (*c*) $St^+ = 1$ and (*d*) $St^+ = 100$; C_0 is the averaged particle concentration defined as the total number of particles with the same St^+ divided by the total volume of the pipe and C is the local particle concentration (number of particles in an annular region divided by its volume). Figure 3(*a*) shows the smooth-wall case, where C/C_0 peaks at the wall, which is the usual case of particle migration due to turbophoresis. Not surprisingly, larger particles tend to migrate more towards the wall because once they are in the low-velocity region close to the wall, due to their large inertia it is difficult for them to leave the wall. As there are few particles in the centre of the pipe for $St^+ = 10$ and 100, the concentration profile is quite low (of $O(10^{-2})$) and therefore noisy.

Particles with very large St^+ (e.g. $St^+ = 1000$) are very sluggish due to the large particle relaxation time and, for the current range of simulation time, are still being transported to the wall.

For the rough-wall case (in figure 3*b*), spikes in concentration are observed for particles with $St^+ = 1$ and 10 within the roughness canopy, as these light particles are trapped in

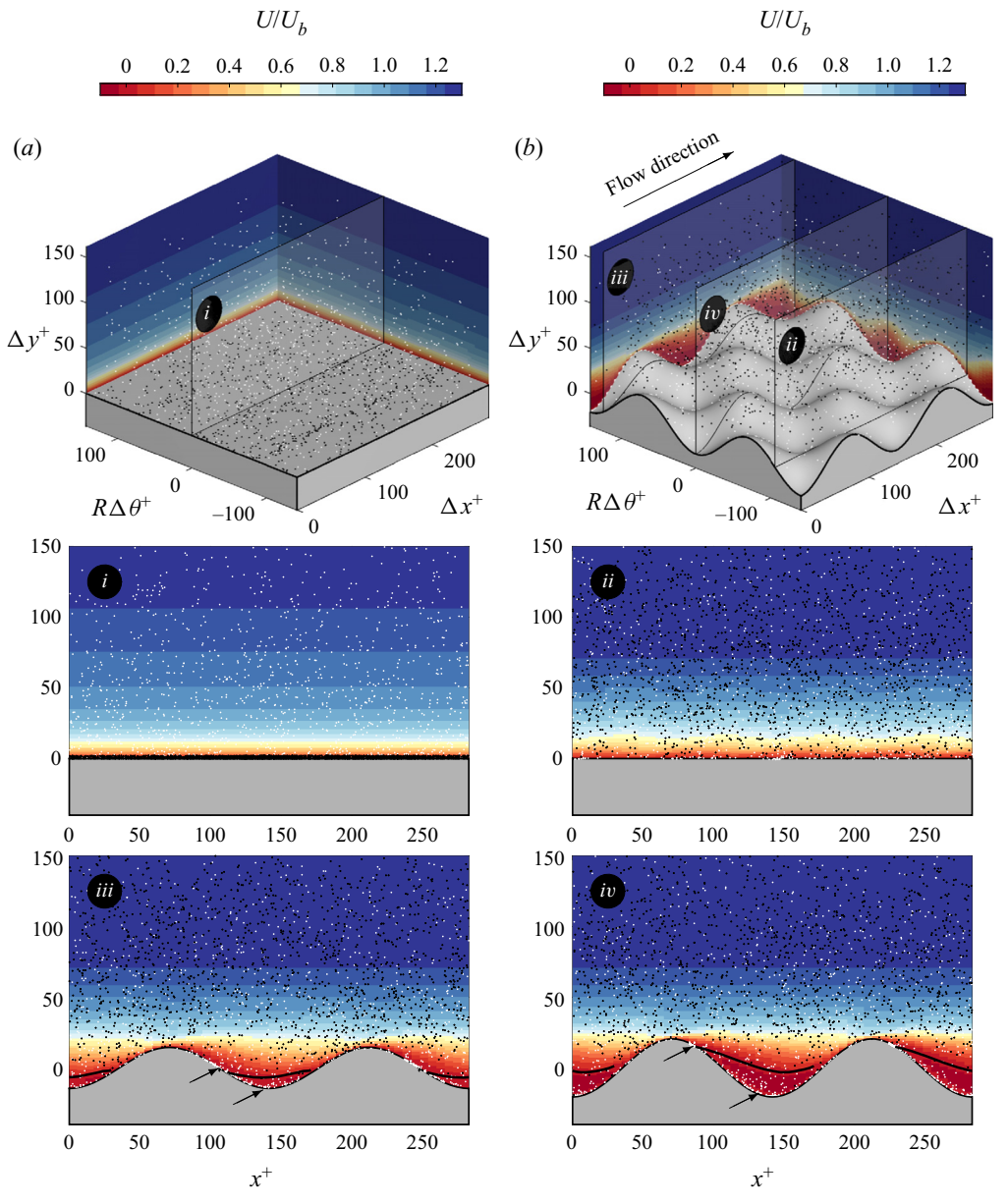

FIGURE 2. Particle distribution of $St^+ = 1$ (in white) and $St^+ = 100$ (in black) for the (*a*) smooth-wall and (*b*) rough-wall cases with $h^+ = 20$ projected onto a flat plane. Coloured contour shows the time-averaged streamwise velocity. Streamwise–wall-normal slices corresponding to the (*i*) smooth wall and the (*ii*, *iii*, *iv*) rough wall at different spanwise locations which are locally smooth and rough. The black line in the roughness canopy show the region where $U^+ = 0$ and the black arrows show the accumulation of $St^+ = 1$ particles.

the wake of the roughness and accumulate on the leeward side and at the trough of the roughness (see figure 2*iii*,*iv*). It is expected that as $t^+ \to \infty$, all of the light particles will accumulate in these regions. Interestingly, for small particles of $St^+ = 1$ (cf. figure 3*c*) no distinct spike in concentration is observed for the rough-wall case with $h^+ = 5$. This is

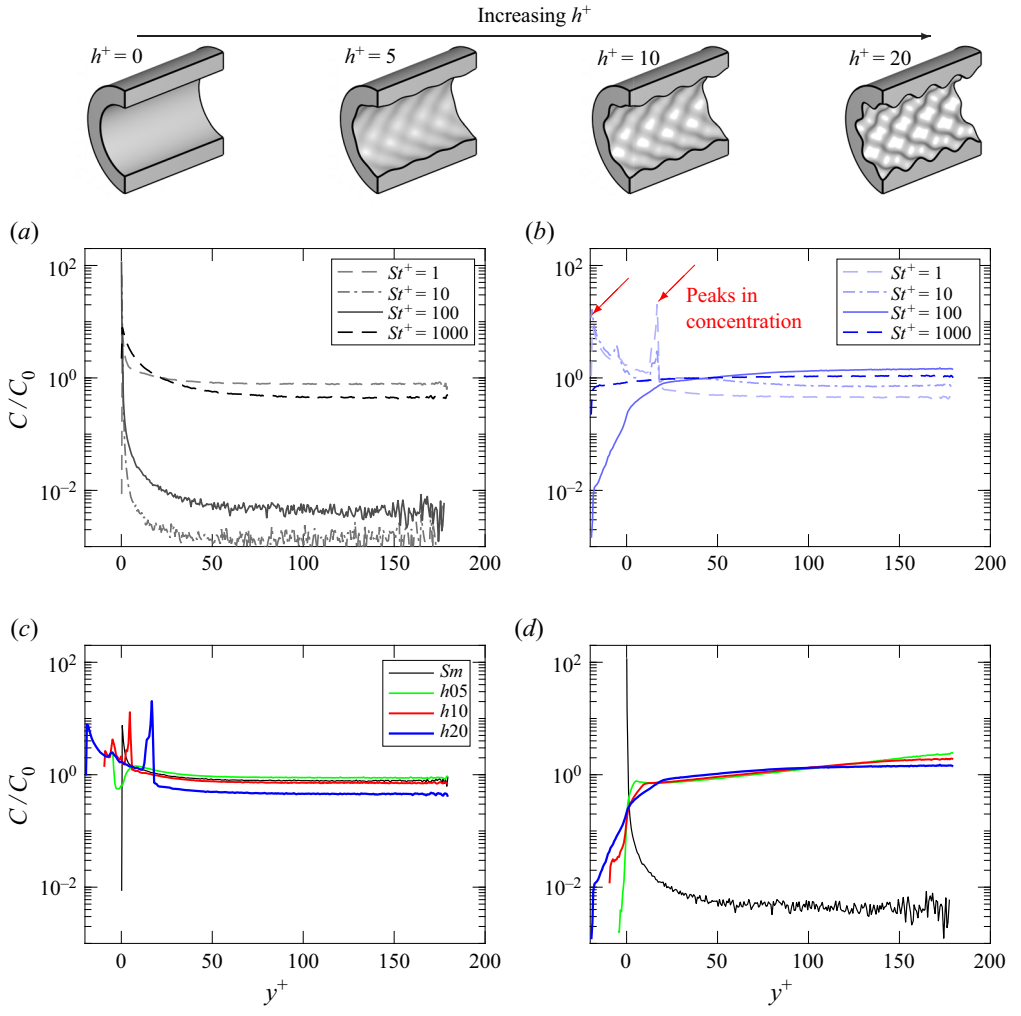

FIGURE 3. Normalised particle concentration against viscous scaled wall-normal height for (*a*) smooth wall and (*b*) rough wall with $h^+ = 20$. Panels (*c*) and (*d*) show the concentration for particles with $St^+ = 1$ and 100, respectively. Red arrows show the peaks in concentration in the roughness canopy. Sketches at the top illustrate the simulated pipes with different roughness heights.

due to the fact that the roughness is not steep enough to cause large flow separation events leeward of the roughness, and hence trap particles.

Inertial particles with large St^+ (cf. figure 3*d*), which would otherwise accumulate to the smooth wall, collide with the rough wall and are distributed throughout the pipe, and lead to $C/C_0 \approx 1$, consistent with the findings of Milici *et al.* (2014). This is also true for the rough-wall case with $h^+ = 5$ despite having a very small roughness height that would typically be considered as a hydrodynamically smooth surface (e.g. Jiménez 2004).

Overall, it is apparent from figure 3 that particle concentration shows distinct features (for varying St^+ and h^+) within the roughness canopy and outside of it (the roughness sublayer). In the following two sections we focus on each of these regions.

4. Roughness canopy

The roughness canopy is the region occupied by the roughness $-h < y < h$ and for the smooth wall is defined as the viscous regime where $0 < y^+ < 5$. This region is important in understanding the deposition mechanism of the particles where numerous experimental and theoretical works have been conducted for the past half a century to predict the deposition velocity and particle collection efficiency (e.g. Liu & Agarwal 1974; Reeks & Skyrme 1976; Guha 1997).

Most studies, however, have been focused on the smooth-wall flows. In the rough-wall case, the particle collection efficiency can be estimated by calculating the mean concentration in the roughness canopy. Figure 4(*a*) shows the contour of the normalised average concentration $\log(C/C_0)$ in the roughness sublayer plotted as a function of h^+ and St^+. The sketches in figure 4(*i–iv*) illustrate the different deposition and resuspension mechanism for smooth and rough walls at different St^+ and h^+ locations as indicated in figure 4(*a*).

Consider the smooth-wall scenario in figure 4(*a*), i.e. $h^+ = 0$, and increasing St^+, i.e. going from (*iii*) to (*iv*) and depicted in the sketches in figure 4(*iii*,*iv*). A cut across this concentration plot is also shown in figure 4(*b*) with a black dashed line. The increasing particle concentration with increasing St^+ is readily evident, and, as mentioned before, is due to the turbophoretic effect. Next, we take $St^+ = 1$, and on 4(*a*) we move vertically from (*iii*) to (*i*). The corresponding schematics are in figure 4(*i*,*iii*). The particle concentration increases with increasing h^+, and this is simply the effect of particles with low inertia getting trapped in the recirculating region occurring behind the roughness 'hills' (see figure 4*c*). However, a slight decrease in concentration occurs at $h^+ = 5$ and this is because there are no recirculating regions due to the small roughness height. The increased velocity in the roughness canopy in fact reduces C compared to the smooth-wall case.

Now, if we increase the St^+ to a 100 and increase h^+ (i.e. from (*iv*) to (*ii*)) going vertically in figure 4(*a*), the concentration decreases. This illustrates the effect of turbophoresis, which tries to bring the particles to the wall, being counteracted by the increasing collision of the particles with the roughness elements that tries to reduce the concentration at the wall. Figure 4(*d*) shows the trajectory of particles with $St^+ = 100$ close to the roughness.

Finally, we see a minimum particle concentration at approximately $St^+ \approx 50$ when we move horizontally at a fixed $h^+ = 20$. This is the location where the particle collision effect (hence reduction in C) overtakes the turbophoresis effect (of increasing C). Various cuts across figure 4(*a*) are shown as lines in figure 4(*b*). The varying trend of C at different h^+ simply quantifies the effects described above.

Results from our regular three-dimensional roughness simulation may provide some insight into the transport and deposition of particles in irregular roughness (due to its practical importance), which contains regions which are locally more or less 'rough' (that could be measured by calculating the local effective slope or roughness parameter). At regions that are locally rough, there will be an increased tendency for particles with small St^+ to accumulate at the wake of roughness and regions of stagnant flow in the roughness canopy. For particles with larger St^+, the wall collision angle would be more acute and would result in more particles travelling against the mean flow as compared to a region which is locally less 'rough'. Although our results provide some suggestions of behaviour over irregular roughness, a full effect requires further investigation.

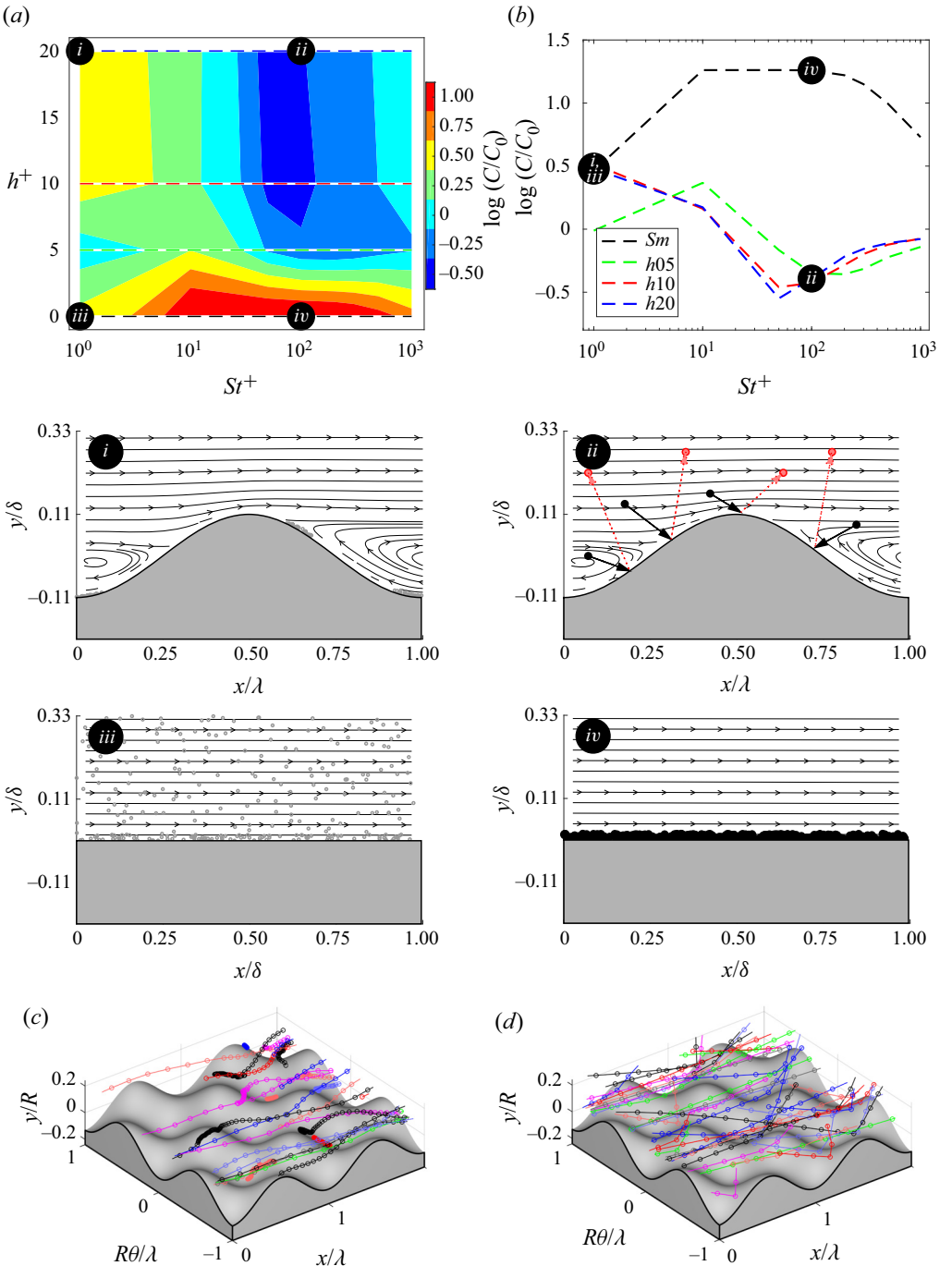

FIGURE 4. Plot of the (*a*) contour of the concentration in the viscous/roughness canopy region and (*b*) the corresponding concentration trends. Sketches (*i*), (*ii*), (*iii*) and (*iv*) illustrate the distribution of particles along the streamwise–wall-normal plane. Particle trajectory close to the rough wall ($h^+ = 20$) for (*c*) $St^+ = 1$ and (*d*) $St^+ = 100$. The time interval between points is $\Delta t^+ = 3.6$, thus, the spacing between points provides an indication of the velocity of the particles.

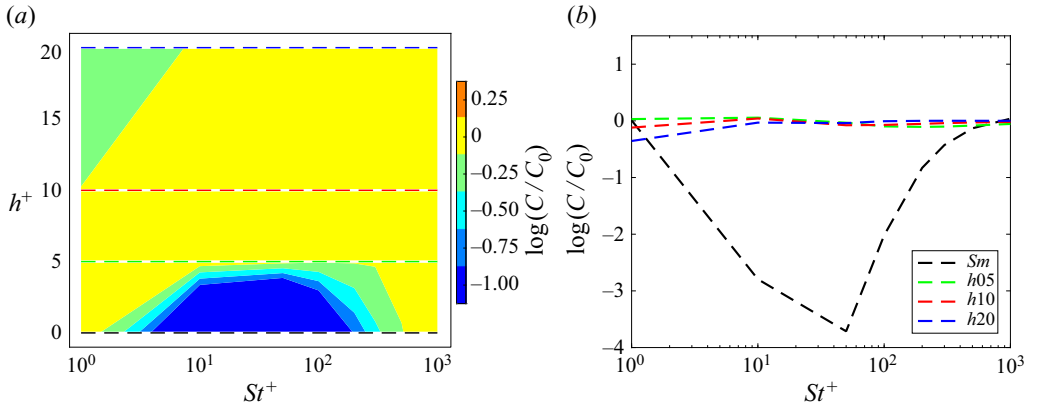

FIGURE 5. Plot of the (*a*) contour of the concentration in the buffer/roughness sublayer region and (*b*) the corresponding concentration trends.

5. Roughness sublayer

The roughness sublayer is the region where the influence of the roughness is felt by the fluid and causes the turbulent statistics for the rough wall to be different from the smooth-wall case. The thickness of the roughness sublayer for these sinusoidal roughnesses is found to scale with the roughness wavelength (Chan *et al.* 2018), and is defined as the region in the range $h < y < \lambda/2$. For the smooth wall, the buffer region is defined as the region in the range $5 < y^+ < 50$.

Figure 5(*a*) shows the $\log(C/C_0)$ plot for the roughness sublayer in a manner similar to figure 4(*a*) for the roughness canopy. Figure 5 is, however, less dramatic, showing decreased regions of C in the two regions (intermediate-St^+/small-h^+ and small-St^+/large-h^+), and this is because most particles have gone to the wall for these parameters. Nevertheless, the interesting feature of the roughness sublayer is that it is an ideal place to observe the effect of roughness generated turbulence on particle velocity and concentration statistics.

In fact, the strong coherent sweep and ejection events by the fluid inside the roughness sublayer play an important part in the transfer mechanism of particles, as suggested by Marchioli & Soldati (2002). They described the transport mechanism of particles in a smooth wall and found that the particle deposition is due to particles accumulating into specific regions in the buffer layer where the coherent structures reside. For a turbulent rough-wall flow, these structures in the roughness sublayer have been modulated by the roughness and the wall effects play an important role.

To understand the dynamics of the particles in the roughness sublayer (or the equivalent buffer region of the smooth wall), the wall-normal velocity of the particles $-u_r^p$ (since this velocity component takes particles towards/away from the wall) is compared with the local fluid velocity sampled by the particle. The momentum transfer of fluid is quantified by the Reynolds stress $-u_x' u_r'^+$, whereas, following Soldati & Marchioli (2009), we consider $-|u_x'|u_r'^+$, where positive values are associated with coherent ejections and negative values are associated with coherent sweeps. Figure 6 shows the joint probability density function (PDF) of $-u_r^p$ against $-|u_x'|u_r'^+$.

Although the turbulent structures for the rough-wall cases differ from the smooth wall, figure 6(*a*) for $St^+ = 1$ is similar because particles are driven towards the wall by sweeping events and are transported away from the wall by ejection events. Probability of these

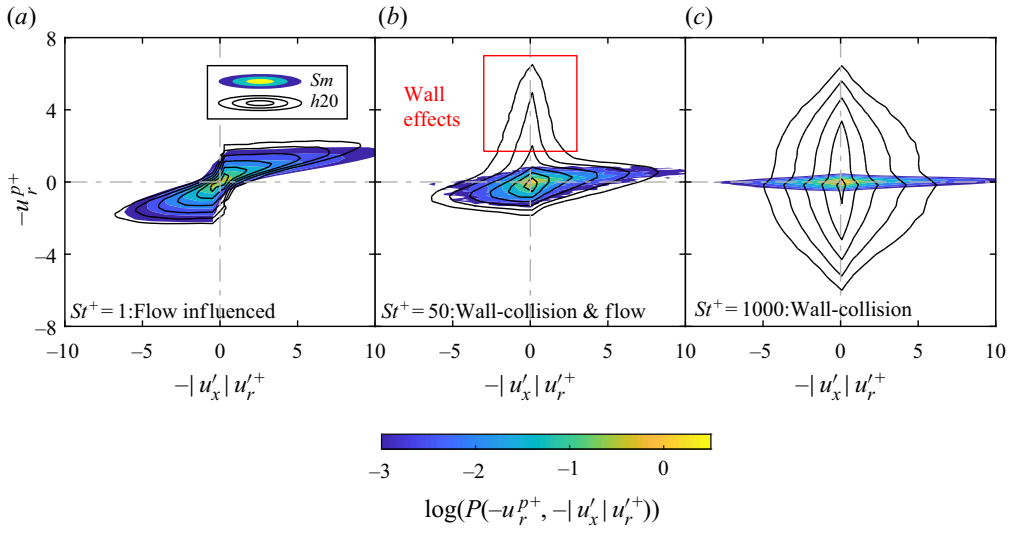

FIGURE 6. Joint PDF of particle wall-normal velocity and coherent fluid events for (*a*) $St^+ = 1$, (*b*) $St^+ = 50$ and (*c*) $St^+ = 1000$ for the smooth wall and rough wall with $h^+ = 20$.

events occurring is presented in table 3. While low St^+ particles act as flow tracers, high St^+ particles filter most of the spectrum of turbulent eddies, such that they are unresponsive to the coherent structures. This is observed in figure 6(*c*) where smooth wall with $St^+ = 1000$ has a smaller range of $-u_r^p$ compared to $St^+ = 1$, although the transport mechanism is still influenced by the sweep and ejection events with probabilities of 55.4 % and 56.8 %, respectively, that are slightly above 50 %. The values of $P \approx 56$ % for sweeps/ejections for $St^+ = 1000$ should be compared to the $P \approx 95$ % for $St^+ = 1$ that is dominated by sweep/ejection events. For $St^+ = 1000$, in comparison with the smooth-wall case, for the rough-wall case in figure 6(*c*), a large scatter in $-u_r^p$ and $-|u_x'|u_r'^+$ is observed with the particles' wall-normal velocity being uncorrelated with the sampling of sweep and ejection events ($P \approx 50$ %). Wall collision is the dominant mechanism, which has no directional preference, and this results in a virtually identical probability of sampling in all four quadrants.

Particles in the intermediate Stokes number are found to be most affected by the dynamics of the buffer region in a smooth-wall pipe (e.g. Picano *et al.* 2009). In the rough-wall pipe, large positive values of $-u_r^p$ are observed in figure 6(*b*) for particles with $St^+ = 50$ due to collision with the wall. The negative $-u_r^p$ region on the other hand has similar trends with $St^+ = 1$ particles, albeit with an increased probability for positive $-|u_x'|u_r'^+$ (ejection) events. At intermediate St^+, these particles are influenced both by the turbulent flow and the wall collisions. The particles with $St^+ = 50$ in the smooth-wall case have all migrated to the wall at this time ($\Delta t^+ = 10\,800$). Therefore, the statistics for this particular St are evaluated at an earlier time ($3600 < \Delta t^+ < 5400$), where the particles are still fleeing the centre towards the wall of the pipe.

Another statistic to consider when analysing the roughness sublayer is the probability density function of the streamwise and wall-normal velocities of both the fluid and the particles. Figure 7 shows the probability distributions of the streamwise and radial velocities normalised by the bulk velocity in the roughness sublayer for all rough and smooth cases.

Smooth wall						
Quadrant	$-u_r^p$	$-\lvert u_x' \rvert u_r'^+$	Event type	$St^+ = 1$	$St^+ = 50$	$St^+ = 1000$
P_I	>0	>0	Ejection	96.9 %	72.6 %	56.8 %
P_{II}	>0	<0	Sweep	3.1 %	27.4 %	43.2 %
P_{III}	<0	<0	Sweep	94.8 %	62.6 %	55.4 %
P_{IV}	<0	>0	Ejection	5.2 %	37.4 %	44.6 %
Rough wall, $h^+ = 20$						
Quadrant	$-u_r^p$	$-\lvert u_x' \rvert u_r'^+$	Event type	$St^+ = 1$	$St^+ = 50$	$St^+ = 1000$
P_I	>0	>0	Ejection	95.0 %	70.0 %	51.0 %
P_{II}	>0	<0	Sweep	5.0 %	30.0 %	49.0 %
P_{III}	<0	<0	Sweep	94.6 %	64.0 %	50.5 %
P_{IV}	<0	>0	Ejection	5.4 %	36.0 %	49.5 %

TABLE 3. Probabilities conditioned on positive or negative particle wall-normal velocity $-u_r^p$ and sweep ($-|u_x'|u_r'^+ < 0$) or ejection events ($-|u_x'|u_r'^+ > 0$) in the buffer/roughness sublayer region. The probabilities are defined as $P_I = P(-|u_x'|u_r'^+ > 0$ and $-u_r^p > 0)$, $P_{II} = P(-|u_x'|u_r'^+ < 0$ and $-u_r^p > 0)$, $P_{III} = P(-|u_x'|u_r'^+ < 0$ and $-u_r^p < 0)$, $P_{IV} = P(-|u_x'|u_r'^+ > 0$ and $-u_r^p < 0)$. Probabilities for the smooth-wall case with $St^+ = 50$ were evaluated at time interval of $3600 < \Delta t^+ < 5400$ ($20 < U_\tau \Delta t/R < 30$).

For particles with a very small Stokes number ($St^+ = 1$ in figure 7*a*,*b*), as one would expect, the $P(u_x/U_b)$ and $P(-u_r/U_b)$ profiles (in dark solid lines) of the particles are similar to the fluid probabilities (in light dashed lines). When the St^+ increases to 50, the probability of the wall-normal velocity (figure 7*d*) is asymmetric as the collision with the rough wall causes particles to bounce away from the wall (i.e. a negative tail), and this effect increases with increasing h^+. After colliding with the wall, the particles become entrained by the bulk flow and only subtle differences between the fluid and particle streamwise velocity probabilities are observed in figure 7(*c*). In this St^+ regime, the particles are not only driven by the turbulent structures of the rough wall but also effected by the wall collision. While the work of Milici *et al.* (2014) concluded that the particle deposition mechanisms between smooth and rough walls are driven by the different turbulent structures, we would argue that the wall collision is also a prominent mechanism for particles with $St^+ = 50$ and higher.

Sluggish, heavy particles with a large Stokes number in figure 7(*f*) on the other hand collide with the rough wall and bounce towards the opposite wall while retaining their inertia to form a symmetric $P(-u_r/U_b)$ profile. As the height of the roughness increases, the steepness of the roughness measured by its 'effective slope' (e.g. Napoli, Armenio & De Marchis 2008), increases. The collision angle becomes more acute and the tendency for the particle trajectory to be in the opposite direction to the mean flow increases with h^+, as observed in the leftward shift of the $P(u_x/U_b)$ profiles in figure 7(*e*).

To reemphasise the above point of particle collision with increasing St^+, we visualise the transport of the particles in different regimes. Five sample particles with $St^+ = 1, 50$ and 1000 in the rough-wall case $h^+ = 20$ are tracked and plotted in figure 8. Only two of the five particles tracks are observed for $St^+ = 1$ (figure 8*a*) as three of the particles are trapped in the roughness canopy. Comparing $St^+ = 50$ particles with $St^+ = 1$ particles, the pathlines of the heavier particles are more aligned with the mean flow and are less

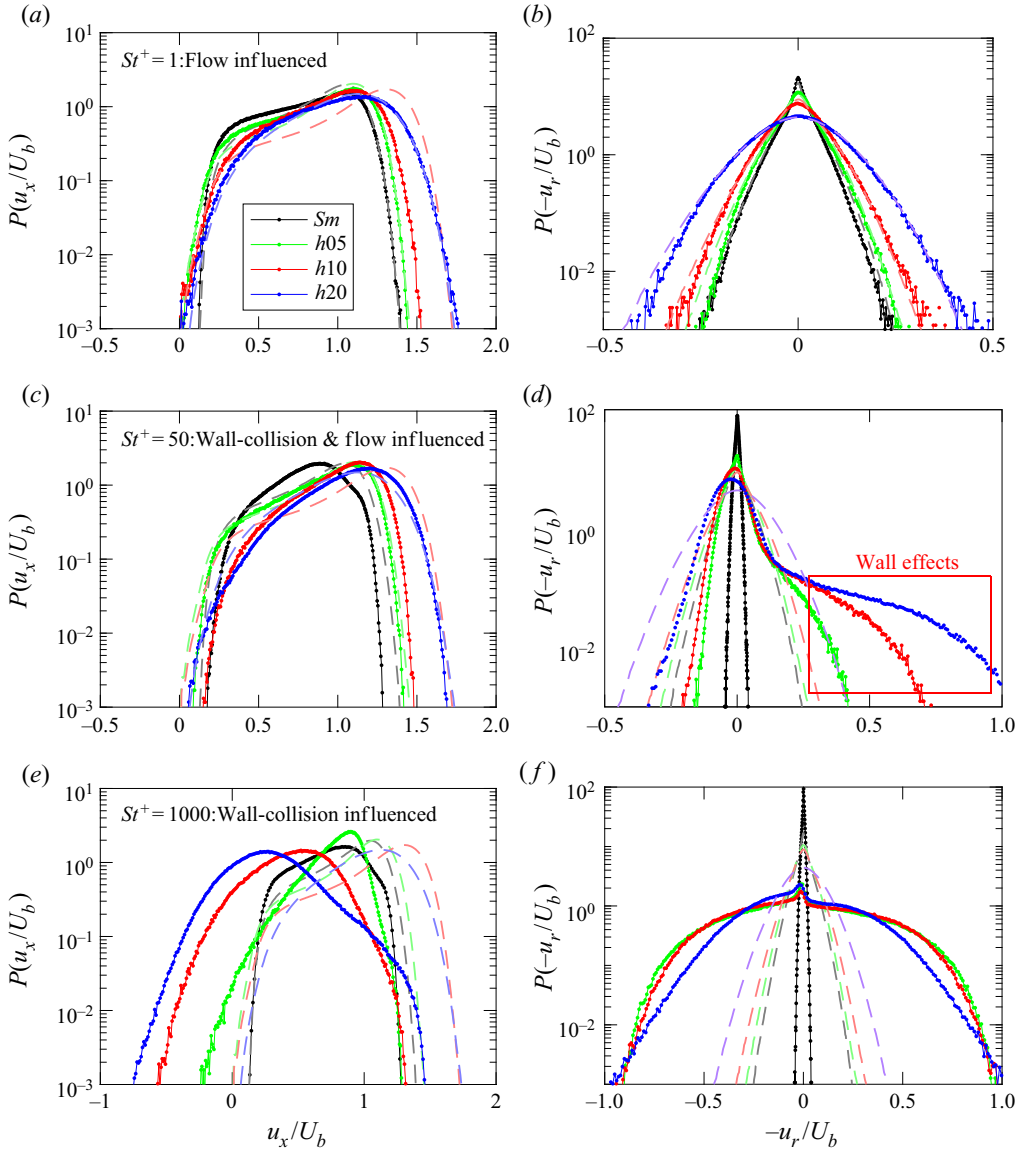

FIGURE 7. Probability density function of the axial (*a*,*c*,*e*) and wall-normal (*b*,*d*,*f*) velocity normalised by the bulk velocity for $St^+ = (a, b)$ 1, (c, d) 50 and (e, f) 1000 in the roughness sublayer/buffer layer. The dashed line shows the probability density function of the sampled fluid velocity.

affected by the sudden turbulent changes in the flow. Collision angle for particles with $St^+ = 50$ is quite shallow compared to $St^+ = 1000$ and the particles are entrained by the bulk flow after bouncing off the wall. Due to the large inertia of particles with $St^+ = 1000$, the trajectories of the particles are almost independent of the flow, and are greatly affected by the roughness topography. The transverse dispersion of the particles and enhanced wall collision frequency due to roughness observed by Kussin & Sommerfeld (2002) in their experimental work are consistent with our observation. Current simulations have been

conducted at a relatively low Reynolds number where there is limited scale separation between the small and large scale structures. At higher Reynolds number, the interactions between the large scale motions and the near-wall small scale structures may affect the transport and deposition mechanism of particles in the smooth-wall pipe, but this remain to be seen.

Having looked at both the roughness canopy and roughness sublayer, in the final part of the results, we now compare the average particle speed within the whole pipe and compare it to the bulk fluid velocities.

6. Average particle motion

The averaged particle velocity in the streamwise direction, $u_b^p = \sum_{i=1}^{N_p} u_{x,i}^p / N_p$ normalised by the fluid bulk velocity, U_b is plotted in figure 9 to quantify the transport of particles in pipes with different roughness heights. This parameter is similar to the particle bulk Reynolds number $Re_b^p = u_b^p \delta/\nu$ which was introduced by Milici *et al.* (2014) but also takes into account the different bulk flow rate of the fluid which decreases with increasing roughness height at a fixed friction Reynolds number.

For convenience, we divide the figure into three regimes; $St^+ = 1$ to 10, 10 to 100 and 100 to 1000. For low St^+ cases (regime *I*), particles in the smooth-wall case have a velocity similar to the fluid. This is of course due to the particles following the fluid almost faithfully. With increasing h^+, u_b^p decreases because more and more light particles get trapped in the roughness canopy where they have reduced velocities. For larger St^+ (regime *II*), the u_b^p for the smooth-wall case drops precipitously due to turbophoresis, which gathers particles at the wall, and where the velocity is close to zero. For rough-wall cases with higher St^+, the trend is opposite, where increasing collisions take the particles way from the wall into the pipe flow region where velocities are higher. For current regular three-dimensional sinusoidal roughness, u_b^p reaches up to 20 % higher than the bulk velocity for case $h^+ = 20$. Interestingly, when $St^+ = 100$, the particles travel on average at a similar velocity as the bulk velocity $u_b^p/U_b \approx 1.07$ for all of the rough cases. With further increase in St^+ (i.e. in regime *III*), u_b^p for all roughness cases reduces. As mentioned before, the effect of turbophoresis becomes important with increasing St^+ and to some extent reduced the particles being taken into the bulk of the pipe, and this in turn brings u_b^p down.

Notice that in figure 9 we include data from the irregular two-dimensional roughness of Milici *et al.* (2014) which also peak in regime *II*. By only looking at the data of Milici *et al.* (2014) one might incorrectly surmise that u_b^p/U_b would asymptote to a constant, and now we see that this need not be the case. The trends for u_b^p/U_b are somewhat roughness topography dependent and the differences between Milici *et al.* (2014) and the current data could also be due to the different flow geometry (pipe vs channel), but it is expected that u_b^p/U_b decreases at the limit $St^+ \to \infty$. This might not be the case if the gravitational force is included, where it is important for particles with large St^+; u_b^p for the smooth-wall flow appears to increase when $St^+ > 100$ but it is because the sluggish particles are still in the core of the pipe and require more time to be transported to the wall (simulation needs to be run for an order of magnitude longer).

Although we can describe the different changes to u_b^p/U_b in figure 9, the situation is not completely satisfactory from a scaling point of view. That is, the different curves for different h^+ seem to peak at different St^+, and one might wonder if the abscissa could be scaled differently (to $St^+ = \tau_p/\tau_f$) to collapse the data and hence reveal a common underlying mechanism. In fact, we know that viscous effects (taken into account by τ_f)

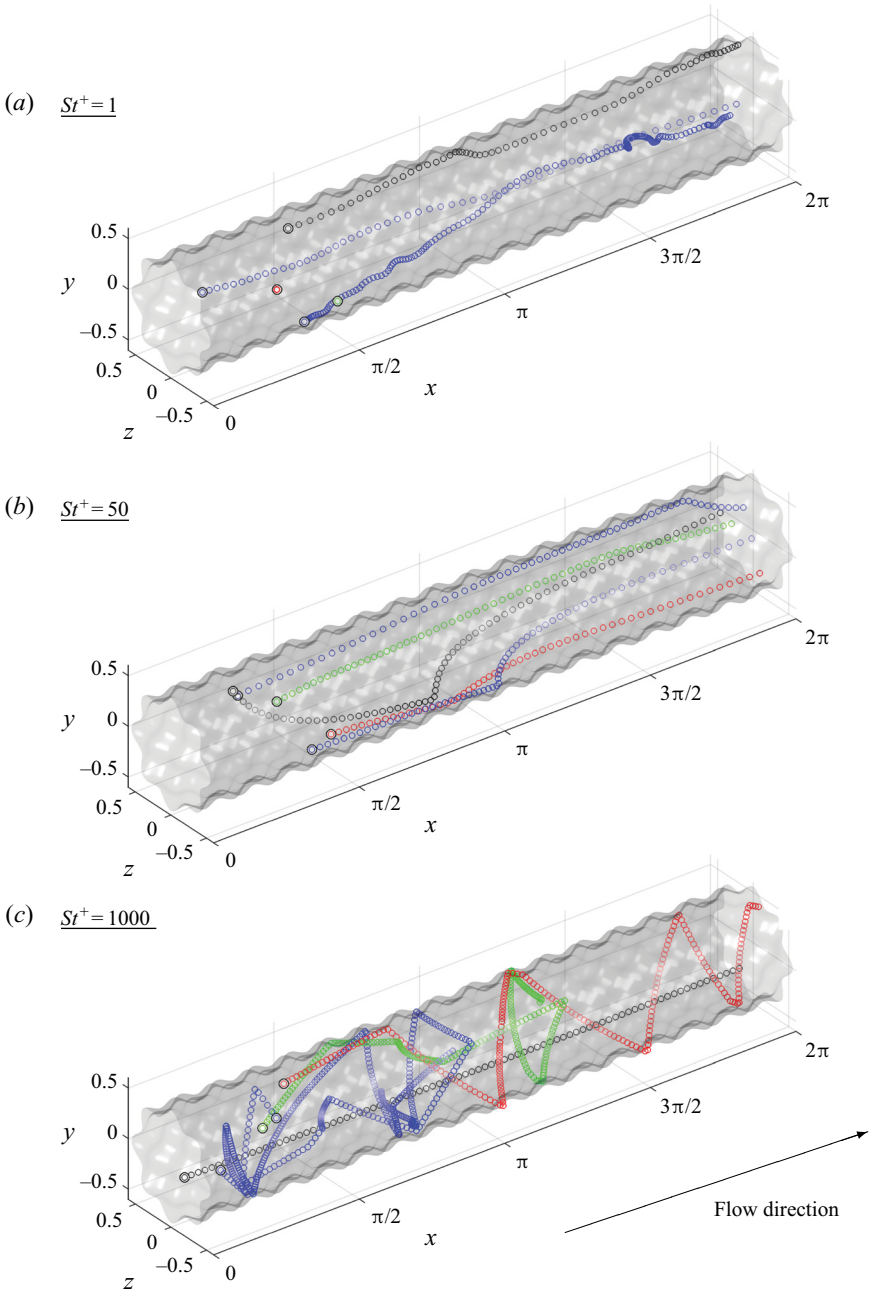

FIGURE 8. Particle tracks for 5 particles with (*a*) $St^+ = 1$, (*b*) 50 and (*c*) 1000 in the rough-wall pipe with $h^+ = 20$. The larger black circle symbol denotes the start of the tracking and particles are shaded from light to dark as a function of the radial location. The time interval between points is $\Delta t^+ = 3.6$, thus, the spacing between points provides an indication of the velocity of the particles.

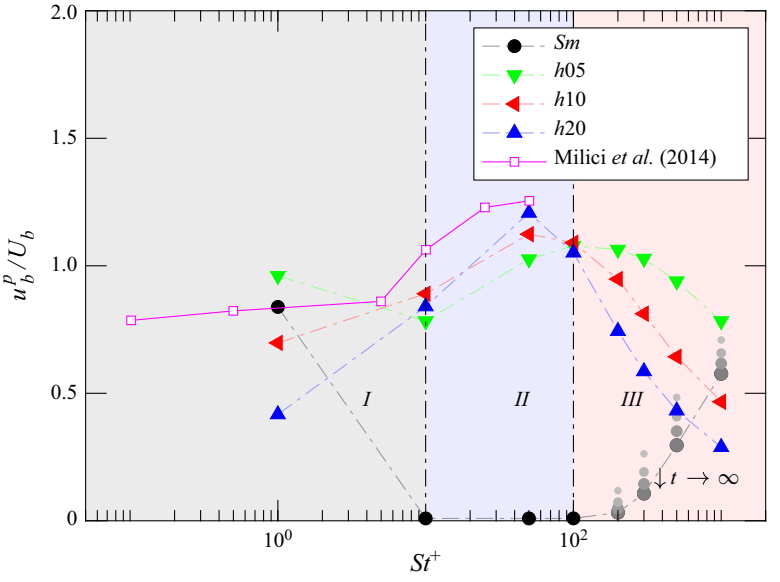

FIGURE 9. Average particle streamwise velocity normalised by the bulk velocity u_b^p/U_b against St^+ for the smooth and rough cases showing the (*I*) flow influenced, (*II*) flow and wall influenced and (*III*) wall influenced regions. Particles of the smooth-wall case with $St^+ > 100$ have not fully converged and are expected $u_b^p \to 0$ as $t \to \infty$. The smaller circular grey symbols are the instantaneous bulk velocities with increasing size corresponding to increased simulation time of $\Delta t^+ = 9000, 10\,800, 12\,600$.

have very little to do with the u_b^p/U_b distribution for roughness cases. Indeed, in plotting figure 9 we neglected any roughness time scale that might play a role. Our roughness has two characteristic length scales, the wavelength λ and roughness height (h). So, apart from the time scales of particles (τ_p) and the viscous effect (τ_f) we introduce a roughness time scale, which could be λ/U_τ or h/U_τ or $(\lambda/h)(\lambda/U_\tau)$. Now, it turns out that if we defined the roughness time scale $\tau_r = (\lambda/h)(\lambda/U_\tau)$, and a Stokes number based on roughness as the particle relaxation time normalised by the roughness time scale $St_r = \tau_p/\tau_r$, the data seem to collapse. Our data of u_b^p/U_b from figure 9 are re-plotted in figure 10 against St_r. This suggests, at least empirically, that both λ and h have an effect on collisions, and hence on u_b^p/U_b. It remains to be seen how u_b^p/U_b changes by varying λ, which is fixed for the present study.

7. Summary and conclusions

A DNS of two-phase flow has been conducted in a turbulent rough-wall pipe with sinusoidal roughness for a range of St^+ and h^+. The transport and deposition mechanisms of the particles in a turbulent rough-wall flow are dependent on the St^+ of the particles and also on some measure of the roughness, which we have chosen to be the roughness height h^+. Three regimes are observed and are elaborated below:

(I) Low St^+: particles with low Stokes numbers (approximately below $St^+ = 10$) behave like tracers and follow the path of the fluid. For very small roughness heights $h^+ = 5$, the flow characteristics of the rough wall are similar to those of the smooth wall and

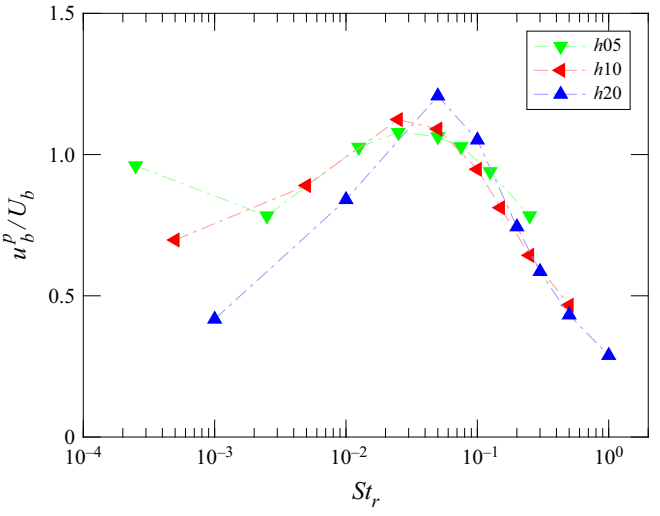

FIGURE 10. Average particle streamwise velocity normalised by the bulk velocity u_b^p/U_b against Stokes roughness number $St_r = \tau_p/\tau_r$ for the smooth and rough cases.

therefore the particle statistics, such as the near-wall concentration, are very similar between the rough and smooth cases. As the roughness becomes more pronounced, changes in the near-wall flow cause these particles to be trapped in the stagnant flow in the trough of the roughness and at the leeward side of the rougness where the flow separates.

(II) Medium St^+: at intermediate Stokes numbers (approximately $10 < St^+ < 100$), the transport mechanism of the particles is balanced by both the turbulent structures of the flow and also collisions with the rough wall. Inertial particles have the tendency to be attracted towards the wall due to turbophoresis. In a turbulent rough-wall flow, the near-wall concentration of particles decreases as the particles are no longer trapped in the roughness canopy but rather collide and bounce off the rough wall. In the roughness sublayer, the particles possess large positive wall-normal velocities due to wall collisionsbut have similar streamwise velocities as the fluid.

(III) High St^+: particles with large Stokes numbers (approximately $St^+ > 100$) are sluggish and the inherent inertia of the particles means that their trajectory is unresponsive to the short time scales of the turbulent flow. The larger the particles' St^+, the larger the turbophoretic effect on the particles, causing a higher frequency of particle collisions with the rough wall. The topography of the roughness becomes important in determining the trajectory and dispersion of the particles as the particle collision angle becomes more acute with increasing roughness slope.

It is important to recall that these results are limited to heavy particles which are small compared to the smallest turbulent scales in the flow and much denser than the carrier phase. In addition, the work here assumes a dilute discrete phase where particle–particle interactions and the back force from the particles on the fluid are not accounted for. A previous study by De Marchis & Milici (2016) has found a decrease in the particle velocity fluctuations when conducting two-way coupling simulations and this could be important for the rough-wall case. These additional parameters would have to be investigated separately in future works.

Acknowledgements

This work was supported by computational resources provided by the Australian Government through NCI and Pawsey under the National Computational Merit Allocation Scheme and also by Pawsey's Energy and Resources Merit Allocation Scheme. The authors gratefully acknowledge the financial support from the Australian Research Council.

Declaration of interests

The authors report no conflict of interest.

Appendix A. Validation of continuous phase

In this section, the mean and turbulent statistics of the continuous phase simulated in OpenFOAM are verified with our previous simulations (Chan *et al.* 2015) which were conducted using CDP, an energy conserving finite volume code (Ham & Iaccarino 2004; Mahesh, Constantinescu & Moin 2004). Figure 11(*a*) shows the mean velocity profiles for the smooth- and rough-wall ($h^+ = 20$) cases at $Re_\tau = 180$ and the profiles from OpenFOAM (OF) lie on top of the profiles from CDP. The second-order statistics for all three velocity components are shown in figure 11(*b*) for the smooth wall and figure 11(*c*) for the rough-wall case. Again, good agreement is observed between CDP and OpenFOAM for both the smooth-wall and rough-wall cases. Within the roughness canopy, the $u^+_{\theta,rms}$ and $u^+_{x,rms}$ profiles of OpenFOAM are slightly lower than CDP although this error is relatively small ($\leq 5\,\%$). The streamwise premultiplied energy spectrum of the streamwise velocity, $k_x\phi^+_{uu}$ is also plotted in figure 11(*d*,*e*) for the smooth- and rough-wall cases, respectively. The black contour lines, which are from the OpenFOAM simulations, agree well with the coloured contours from the CDP simulations. This indicates that the OpenFOAM is able to resolve all of the turbulent scales in the flow (with sufficient mesh resolution) and is capable of conducting DNS type simulations.

Appendix B. Saffman–Mei lift force on particle distribution

Here, we investigate the effects of Saffman lift force on the distribution of particles in a turbulent rough-wall pipe flow. The Saffman lift force acts to migrate particles in a shear flow across streamlines. Since the original derivation was for particles in a Poiseuille flow (Saffman 1956), empirical corrections have formed the basis of advancing the lift force to include Reynolds number effects. In this study, we use the Saffman–Mei lift force (Mei 1992)

$$F_L = m_p \frac{\rho}{\rho_p} C_L((\boldsymbol{u} - \boldsymbol{u}^p) \times \boldsymbol{\omega}_f), \tag{B 1}$$

which will be the additional term added to the right-hand side of (2.4). It can be seen that the contribution of the lift force is less effective in the limit of high particle to fluid density ratios and is therefore often neglected (Peker & Helvaci 2011); $\boldsymbol{\omega}_f$ is the vorticity of the fluid at the location of the point particle, and C_L is calculated from the following equations:

$$C_L = \frac{3}{2\pi\sqrt{Re_s}} C_{LS}, \tag{B 2}$$

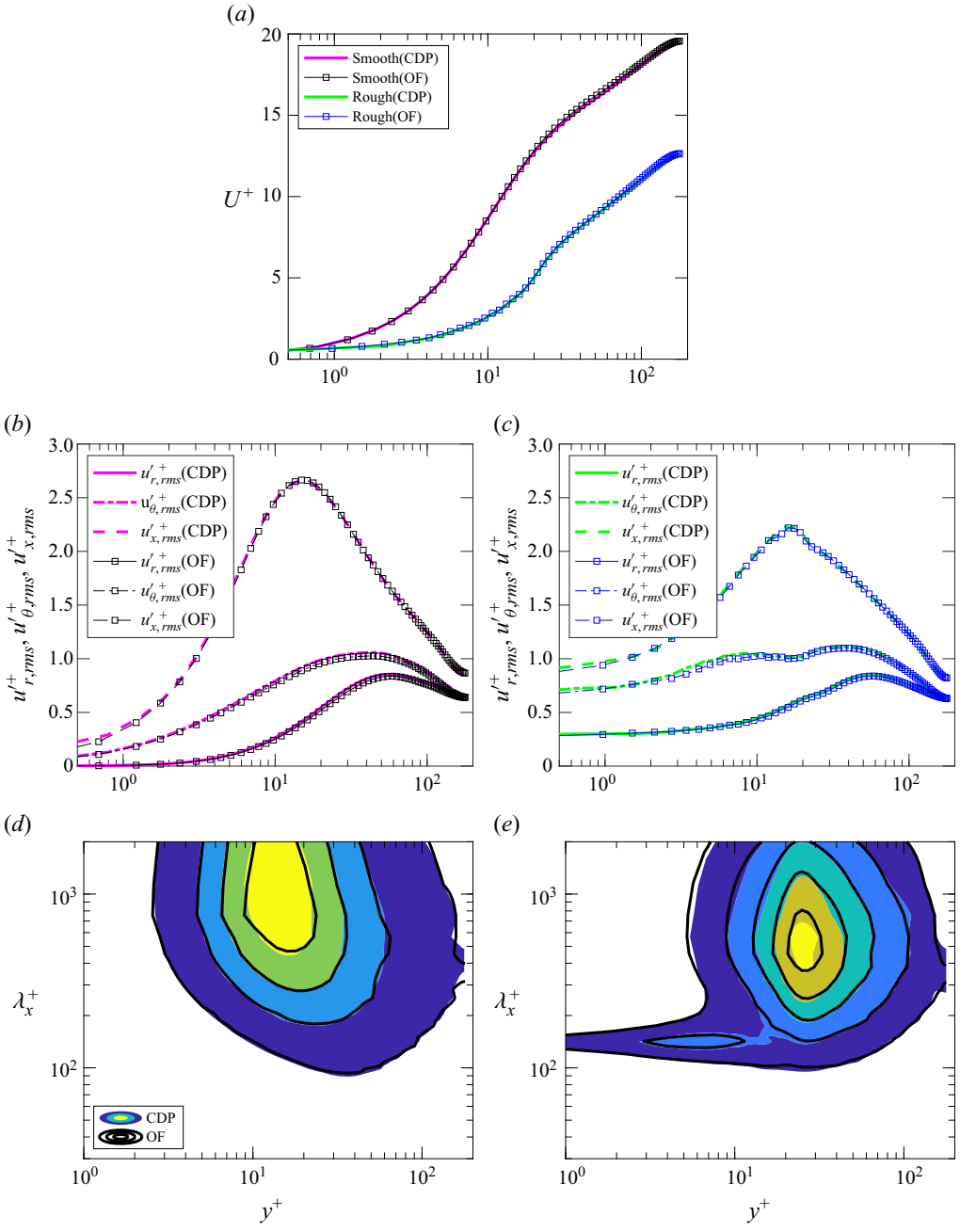

FIGURE 11. Plot of the (*a*) mean velocity profile, second-order statistics for the (*b*) smooth- and (*c*) rough-wall ($h^+ = 20$) cases at $Re_\tau = 180$. Contours of the streamwise premultiplied energy spectra of the streamwise velocity, $k_x\phi^+_{uu}$ for (*d*) smooth wall and (*e*) rough wall. Contour levels start at 0.25 with increments of 0.5 for the smooth wall and 0.25 for the rough wall.

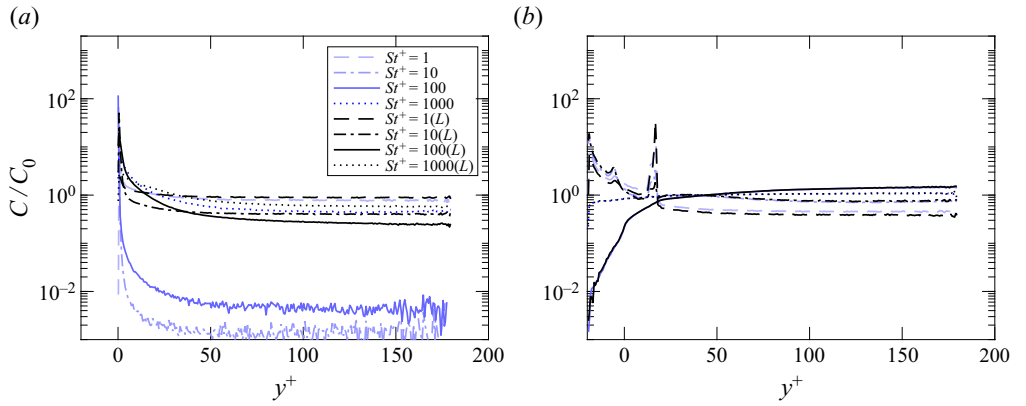

FIGURE 12. Normalised particle concentration against viscous scaled wall-normal height for the (*a*) smooth- and (*b*) rough-wall ($h^+ = 20$) cases for particles with (*L*) and without the Saffman–Mei lift force.

where

$$C_{LS} = \begin{cases} 6.46f & \text{if } Re_p < 40 \\ 6.46 \cdot 0.0524\sqrt{\beta Re_p} & \text{if } Re_p \geq 40 \end{cases} \tag{B 3}$$

and $Re_s = d_p^2|\boldsymbol{\omega}_f|/\nu$, $\beta = \frac{1}{2}(Re_s/Re_p)$, $f = (1-\alpha)\exp(-0.1Re_p) + \alpha$, $\alpha = 0.3314\sqrt{\beta}$. The direction of this force depends on the sign of the slip velocity. In a smooth-wall flow with inertial particles, the Saffman lift force first enhances migration towards the walls as particles that have gained high velocities in the turbulent core enter lower-velocity fluid regions close to the wall. In an application where particles rebound from solid walls, particles that lag the fluid will experience a lift force that assists in their migration away from the viscous sub-layer, where the influence of lift is significant (Zheng & Silber-Li 2009; Costa *et al.* 2020). In a rough-wall flow, the contribution of this phenomenon is expected to be less important, as alternate re-entrainment mechanisms exist.

While there is a significant difference in the concentration profiles close to the smooth wall (figure 12*a*), the effects of the Saffman–Mei lift force on the distribution of the particles in the rough-wall pipe ($h^+ = 20$) are negligible (figure 12*b*). For particles with large St^+, where the lift forces are expected to be important in the near-wall region, the particle concentration profiles in the rough-wall pipe are in good agreement. This is because the particle wall collision is the main transport mechanism.

REFERENCES

AMBROSINO, F. 2011 Wall effects in particle-laden flows. PhD thesis, University of Naples Federico II, Naples, Italy.

ARMENIO, V. & FIOROTTO, V. 2001 The importance of the forces acting on particles in turbulent flows. *Phys. Fluids* **13**, 2437–2440.

BAGCHI, P. & BALACHANDAR, S. 2004 Response of the wake of an isolated particle to an isotropic turbulent flow. *J. Fluid Mech.* **518**, 95–123.

BALACHANDAR, S. & EATON, J. K. 2010 Turbulent dispersed multiphase flow. *Annu. Rev. Fluid Mech.* **42**, 111–133.

BENSON, M., TANAKA, T. & EATON, J. K. 2004 Effects of wall roughness on particle velocities in a turbulent channel flow. *Trans. ASME: J. Fluids Engng* **127**, 250–256.

BURTON, T. M. & EATON, J. K. 2005 Fully resolved simulations of particle-turbulence interaction. *J. Fluid Mech.* **545**, 67–111.

CHAN, L., MACDONALD, M., CHUNG, D., HUTCHINS, N. & OOI, A. 2015 A systematic investigation of roughness height and wavelength in turbulent pipe flow in the transitionally rough regime. *J. Fluid Mech.* **771**, 743–777.

CHAN, L., MACDONALD, M., CHUNG, D., HUTCHINS, N. & OOI, A. 2018 Secondary motion in turbulent pipe flow with three-dimensional roughness. *J. Fluid Mech.* **854**, 5–33.

CHANG, Y. & SCOTTI, A. 2003 Entrainment and suspension of sediments into a turbulent flow over ripples. *J. Turbul.* **4**, 1–22.

CHIN, C., OOI, A., MARUSIC, I. & BLACKBURN, H. M. 2010 The influence of pipe length on turbulence statistics computed from direct numerical simulation data. *Phys. Fluids* **22**, 115107.

COCEAL, O., DOBRE, A., THOMAS, T. G. & BELCHER, S. E. 2007 Structure of turbulent flow over regular arrays of cubical roughness. *J. Fluid Mech.* **589**, 375–409.

COSTA, P., BRANDT, L. & PICANO, F. 2020 Interface-resolved simulations of small inertial particles in turbulent channel flow. *J. Fluid Mech.* **883**, A54–1–A54–19.

DE MARCHIS, M. & MILICI, B. 2016 Turbulence modulation by micro-particles in smooth and rough channels. *Phys. Fluids* **28** (11), 115101.

DE MARCHIS, M., MILICI, B., SARDINA, G. & NAPOLI, E. 2016 Interaction between turbulent structures and particles in roughened channel. *Intl J. Multiphase Flow* **78**, 117–131.

FESSLER, J. R., KULICK, J. D. & EATON, J. K. 1994 Preferential concentration of heavy particles in a turbulent channel flow. *Phys. Fluids* **6**, 3742–3749.

GUHA, A. 1997 A unified Eulerian theory of turbulent deposition to smooth and rough surfaces. *J. Aerosol Sci.* **28**, 1517–1537.

HAM, F. & IACCARINO, G. 2004 Energy conservation in collocated discretization schemes on unstructured meshes. In *CTR Annual Research Briefs*, pp. 3–14.

HAMILTON, J. M., KIM, J. & WALEFFE, F. 1995 Regeneration mechanisms of near-wall turbulence structures. *J. Fluid Mech.* **287**, 317–348.

JIMÉNEZ, J. 2004 Turbulent flows over rough walls. *Annu. Rev. Fluid Mech.* **36**, 173–196.

KÄRRHOLM, F. P. 2006 Rhie-Chow interpolation in OpenFOAM. Department of Applied Mechanics, Chalmers University of Technology.

KONAN, N. A., KANNENGIESER, O. & SIMONIN, O. 2009 Stochastic modeling of the multiple rebound effects for particle–rough wall collisions. *Intl J. Multiphase Flow* **35**, 933–945.

KROGSTAD, P.-Å. & ANTONIA, R. A. 1994 Structure of turbulent boundary layers on smooth and rough walls. *J. Fluid Mech.* **277**, 1–21.

KULICK, J. D., FESSLER, J. R. & EATON, J. K. 1994 Particle response and turbulence modification in fully developed channel flow. *J. Fluid Mech.* **277**, 109–134.

KUSSIN, J. & SOMMERFELD, M. 2002 Experimental studies on particle behaviour and turbulence modification in horizontal channel flow with different wall roughness. *Exp. Fluids* **33**, 143–159.

LIU, B. Y. H. & AGARWAL, J. K. 1974 Experimental observation of aerosol deposition in turbulent flow. *J. Aerosol Sci.* **5**, 145–155.

MACDONALD, M., CHAN, L., CHUNG, D., HUTCHINS, N. & OOI, A. 2016 Turbulent flow over transitionally rough surfaces with varying roughness densities. *J. Fluid Mech.* **804**, 130–161.

MAHESH, K., CONSTANTINESCU, G. & MOIN, P. 2004 A numerical method for large-eddy simulation in complex geometries. *J. Comput. Phys.* **197**, 215–240.

MARCHIOLI, C. & SOLDATI, A. 2002 Mechanisms for particle transfer and segregation in a turbulent boundary layer. *J. Fluid Mech.* **468**, 283–315.

MAXEY, M. R. & RILEY, J. J. 1983 Equation of motion for a small rigid sphere in a nonuniform flow. *Phys. Fluids* **26** (4), 883–889.

MEI, R. 1992 An approximate expression for the shear lift force on a spherical particle at finite Reynolds number. *Intl J. Multiphase Flow* **18** (1), 145–147.

MILICI, B., DE MARCHIS, M., SARDINA, G. & NAPOLI, E. 2014 Effects of roughness on particle dynamics in turbulent channel flows: a DNS analysis. *J. Fluid Mech.* **739**, 465–478.

NAPOLI, E., ARMENIO, V. & DE MARCHIS, M. 2008 The effect of the slope of irregularly distributed roughness elements on turbulent wall-bounded flows. *J. Fluid Mech.* **613**, 385–394.

OLIVEIRA, J. L. G., VAN DER GELD, C. W. M. & KUERTEN, J. G. M. 2017 Concentration and velocity statistics of inertial particles in upward and downward pipe flow. *J. Fluid Mech.* **822**, 640–663.

ORLANDI, P. & LEONARDI, S. 2006 DNS of turbulent channel flows with two- and three-dimensional roughness. *J. Turbul.* **7**, 1–22.

PEKER, S. M. & HELVACI, S. S. 2011 *Solid-Liquid Two Phase Flow*. Elsevier.

PICANO, F., SARDINA, G. & CASCIOLA, C. M. 2009 Spatial development of particle-laden turbulent pipe flow. *Phys. Fluids* **21**, 093305.

PUTNAM, A. 1961 Integratable form of droplet drag coefficient. *ARSJ-Am. Rocket Soc. J.* **31**, 1467–1468.

REEKS, M. W. 1983 The transport of discrete particles in inhomogeneous turbulence. *J. Aerosol Sci.* **14**, 729–739.

REEKS, M. W. & SKYRME, G. 1976 The dependence of particle deposition velocity on particle inertia in turbulent pipe flow. *J. Aerosol Sci.* **7**, 485–495.

RHIE, C. M. & CHOW, W. L. 1983 Numerical study of the turbulent flow past an airfoil with trailing edge separation. *AIAA J.* **21**, 1525–1532.

ROUSON, D. W. I. & EATON, J. K. 2001 On the preferential concentration of solid particles in turbulent channel flow. *J. Fluid Mech.* **428**, 149–169.

SAFFMAN, P. G. 1956 On the motion of small spheroidal particles in a viscous liquid. *J. Fluid Mech.* **1** (5), 540–553.

SARDINA, G., SCHLATTER, P., BRANDT, L., PICANO, F. & CASCIOLA, C. M. 2012*a* Wall accumulation and spatial localization in particle-laden wall flows. *J. Fluid Mech.* **699**, 50–78.

SARDINA, G., SCHLATTER, P., PICANO, F., CASCIOLA, C. M., BRANDT, L. & HENNINGSON, D. S. 2012*b* Self-similar transport of inertial particles in a turbulent boundary layer. *J. Fluid Mech.* **706**, 584–596.

SOLDATI, A. & MARCHIOLI, C. 2009 Physics and modelling of turbulent particle deposition and entrainment: review of a systematic study. *Intl J. Multiphase Flow* **35**, 827–839.

SOMMERFELD, M. 1992 Modelling of particle-wall collisions in confined gas-particle flows. *Intl J. Multiphase Flow* **18**, 905–926.

SOMMERFELD, M. & HUBER, N. 1999 Experimental analysis and modelling of particle-wall collisions. *Intl J. Multiphase Flow* **25**, 1457–1489.

UIJTTEWAAL, W. S. J. & OLIEMANS, R. V. A. 1996 Particle dispersion and deposition in direct numerical and large eddy simulations of vertical pipe flows. *Phys. Fluids* **8** (10), 16.

VOLINO, R. J., SCHULTZ, M. P. & FLACK, K. A. 2007 Turbulence structure in rough-and smooth-wall boundary layers. *J. Fluid Mech.* **592**, 263–293.

VREMAN, A. W. 2007 Turbulence characteristics of particle-laden pipe flow. *J. Fluid Mech.* **584**, 235–279.

WELLER, H. G., TABOR, G., JASAK, H. & FUREBY, CHRISTER 1998 A tensorial approach to computational continuum mechanics using object-oriented techniques. *Comput. Phys.* **12**, 620–631.

YOUNG, J. & LEEMING, A. 1997 A theory of particle deposition in turbulent pipe flow. *J. Fluid Mech.* **340**, 129–159.

ZHENG, X. & SILBER-LI, Z. 2009 The influence of saffman lift force on nanoparticle concentration distribution near a wall. *Appl. Phys. Lett.* **95** (12), 124105.